Applied Catalysis B: Environmental 136–137 (2013) 202–209

Contents lists available at SciVerse ScienceDirect

Applied Catalysis B: Environmental

journal homepage: www.elsevier.com/locate/apcatb

# The impact of ZnO load, stability and morphology on the kinetics of the photocatalytic degradation of caffeine and resazurin

Marko Bitenc[a,b], Barbara Horvat[c,d], Blaž Likozar[b], Goran Dražić[c,d], Zorica Crnjak Orel[a,b,*]

[a] Center of Excellence for Polymer Materials and Technologies, Tehnološki park 24, SI-1000 Ljubljana, Slovenia
[b] National Institute of Chemistry Slovenia, Hajdrihova 19, SI-1001 Ljubljana, Slovenia
[c] Jožef Stefan Institute, Jamova 39, SI-1000, Ljubljana, Slovenia
[d] Jožef Stefan International Postgraduate School, Jamova 39, SI-1000, Ljubljana, Slovenia

ARTICLE INFO

*Article history:*
Received 23 October 2012
Received in revised form 25 January 2013
Accepted 1 February 2013
Available online 15 February 2013

*Keywords:*
Photocatalysis
ZnO
Hydrozincite
Kinetics
Band gap

ABSTRACT

Zinc oxide (ZnO) powders with diverse morphologies were synthesized with various solvothermal techniques. Water, 1-butanole and ethylene glycol were used as the solvents, while the temperature of the solvothermal synthesis was varied from 90 °C to 120 °C. Resazurin and caffeine were used for the evaluation of the photocatalytic activity of all the prepared samples, and in particular to compare ZnO with commercial titanium dioxide photocatalytic material (P25 Evonik Degussa) using UV–vis spectroscopy. The composition, crystallinity, and morphology of the prepared materials were investigated with FTIR, XRD, TEM and FEG-SEM techniques. The band gaps of the obtained semiconductors were measured because the band gap of hydrozincite, determined in this study to be 4.1 eV, has not been reported previously. The specific surface area (BET) and the porosity of the prepared particles were estimated. The crystal size in one dimension was estimated and was found to play an important role in the photocatalytic activity, which increased with a smaller size. A higher degree of aggregation caused the opposite effect. Thus, a more aggregated material with a larger surface area than a less aggregated one exhibited a lower photocatalytic activity. The particle morphology strongly influenced the photocatalytic process, while the degree of crystallinity was not comparably significant. The external mass-transfer (diffusion to the catalytic surface) resistance was negligible, and consequently the first-order, second-order, and Langmuir–Hinshelwood mechanism kinetics of the photocatalysis were examined.



## 1. Introduction

ZnO is a direct-band-gap semiconductor with an energy gap of 3.37 eV [1,2]. This value is very close to the highly photocatalytic anatase $TiO_2$, which has a band gap of 3.21 eV [3]. As a result, ZnO seems to be a promising alternative for the degradation of organic pollutants in water. Literature data relating to its photocatalytic properties can be found in several articles [1,2,4–7]. Márquez et al. [1] showed that the ZnO particles' grain number and grain size on the substrate had to be optimized for the best photocatalytic effect. Lai et al. [2] confirmed the existence of several kinds of defects in as-prepared, flower-like ZnO powders. However, they found that only the oxygen vacancy showed a very positive correlation with the photocatalytic activity of ZnO materials. Li and Haneda [4] dealt with the dependence of photocatalysis on the morphology and they found that it has a large impact on the photocatalysis and that the crystallinity is more important than the ZnO surface itself. However, ongoing research is dedicated to the development of different ZnO morphologies with enhanced properties to treat organic pollutants and help to understand the various contributions to the overall pollutant-decomposition rate.

In order to model, optimize and scale-up the photocatalytic processes, the roles of the hydrodynamics, mass transfer and kinetics have to be understood. For the kinetics of photocatalytic reactions with zinc oxide the Langmuir-Hinshelwood mechanism was most often employed [8–13]. On the other hand, Vora et al. [7] and Yatmaz et al. [14] used a simple, first-order, decomposition model; however, this corresponds to a specific case of the Langmuir–Hinshelwood mechanism when either the adsorption constant or the adsorbate concentration is low [8–11]. Kumar et al. [15] proposed that rather than the equilibrium [8,13] or initial [9,10,12] concentration of the adsorbate, a transient concentration should be used. To determine the intrinsic kinetics the absence of mass-transfer limitations has to be confirmed. This is seldom done, even though mass transfer may be the reason for the apparent first-order kinetics [7–15].

* Corresponding author at: National Institute of Chemistry Slovenia, Hajdrihova 19, SI-1001 Ljubljana, Slovenia. Tel.: +386 1 4760236; fax: +386 1 4760300.
*E-mail address:* zorica.crnjak.orel@ki.si (Z.C. Orel).

0926-3373/$ – see front matter © 2013 Elsevier B.V. All rights reserved.
http://dx.doi.org/10.1016/j.apcatb.2013.02.016

In this paper various ZnO particle morphologies are presented, obtained with different syntheses, in order to test the dependence of the photocatalytic activity on these morphologies. The band gaps of the synthesized semiconductors were determined, with the one relating to hydrozincite being established for the first time. Furthermore, the photocatalytic effect for caffeine and resazurin was described using kinetic calculations, acknowledging the effect of the ZnO load, stability, and morphology.

## 2. Experimental

### 2.1. ZnO preparation

In a typical experimental procedure the chemicals used were dissolved in Milli-Q water to provide a fresh stock solution and avoid hydrolysis during storage. The chemicals were analytical reagents and used without any further purification. Three types of sample preparation were performed.

The first set of experiments was carried out in two steps. The first step of the sample preparation (marked as **sample A**) involved hydrothermal precipitation in 500-ml laboratory bottles, which were placed in a preheated oven at 90 °C for 24 h. For this reaction, we dissolved 16.97 mmol of zinc nitrate hexahydrate (Sigma–Aldrich, 98%) and 84.91 mmol of urea (Sigma–Aldrich, 99%) in 425 ml of Milli-Q water. The as-prepared precipitate was cooled to room temperature, filtered off, washed with water and dried in air. In the second step, the as-prepared solids were thermally treated in a preheated oven at 300 °C for 1 hour. The obtained product is marked as **sample TA**.

The second set of samples (marked as **sample B**) was prepared in 500-ml laboratory bottles that were placed in an oven preheated at 120 °C for 24 h. For this reaction, 60.88 mmol of zinc acetylacetonate hydrate powder (Sigma–Aldrich) were dispersed in 425 ml of 1-butanole (Sigma–Aldrich). The as-prepared solids were centrifuged for 10 min at 10,000 rpm, washed with absolute ethanol three times and dried in air.

The third set of samples (marked as **sample C**) was prepared with constant stirring (250 rpm) in a 500-ml open reactor at 90 °C for 24 h. For this reaction, 19.97 mmol of zinc nitrate hexahydrate (Sigma–Aldrich, 98%) and 84.91 mmol of urea (Sigma–Aldrich, 99%) were dissolved in 400 ml of the reaction mixture of Milli-Q water and ethylene glycol (EG, Merck) with a volume ratio of 1/3. The as-prepared solids were filtered off, washed with water and dried in air.

### 2.2. Photocatalysis

The photocatalytic effects of the prepared materials, and the Degussa P25 were tested with the blue oxidized redox dye **resazurin** (Sigma–Aldrich, 92% of dye content) and **caffeine** (Sigma–Aldrich, 99%). Resazurin was prepared from 600 mg of aqueous polymer hydroxyethyl-cellulose (Sigma–Aldrich), 89.4 g of Milli-Q water, 100 mg of the resazurin powder and 4 g of the sacrificial electron donor glycerol (Sigma–Aldrich). The solution of caffeine was prepared by dissolving 245 mg caffeine in 50 ml of Milli-Q water. The ingredients were stirred for 1 h to ensure their thorough dissolution.

The photocatalytic experiments were carried out in an **incubator** (with cooling ability from the company Kambič (Slovenia), type I-265 CKUV). In the incubator two different lights were used simultaneously, i.e., two Osram L18/73 bulbs (Gaussian spectrum from 300 nm to 400 nm with a peak at approximately 375 nm) and one 300-W Ultra Vitalux lamp with a solar spectrum without UVC.

The formulation of resazurin or caffeine was added to 100 ml of Milli-Q water and 40 mg of pre-sonicated, prepared powder sample. Sonication had no effect other than the de-aggregation of the photocatalyst, as temperature was maintained at the ambient conditions. The concentrations of resazurin and caffeine were 10.6 mg $L^{-1}$ ($1.06 \times 10^{-3}$ wt.%) and 48.9 mg $L^{-1}$ ($4.89 \times 10^{-3}$ wt.%), respectively. The suspension was constantly stirred at 20 °C and irradiated. A total of 2 ml out of 100 ml of radiated suspension was sampled at 0 min (10 min of stirring under darkness), and consequently every 10 min, or later 30 min, during the irradiation, centrifuged at 13,000 rpm for 20 min, which was followed by removal of the supernatant.

### 2.3. Characterization

The band gap and the photocatalytic activity were determined from the UV–vis spectra measured with PerkinElmer's Lambda 950 spectrophotometer with a 150-mm sphere in the ranges from 250 nm to 800 nm and 225 nm to 350 nm for the resazurin and caffeine, respectively. Although the process could have been followed by high-performance liquid chromatography to avoid the problem of the overlapping spectra for caffeine, [12] UV–vis spectroscopy, combined with peak deconvolution, is a faster, and in this case, equally reliable measuring technique [7–11,13–15]. When determining the band gap from the absorbance spectrum $A(\lambda)$, where $A$ is the absorbance and $\lambda$ is the wavelength of the source light, we transformed the measurement into $[A(\hbar\omega) \cdot \hbar\omega]^2$, where $\hbar = h/2\pi$, with h being Planck's constant and $\omega$ the angular frequency. The obtained characteristic curves could be divided in two almost linear regions (at the initial and final parts of the curve). The projection onto the $x$-axis of the intersection of the linear extrapolations of both linear regions was used to determine the band-gap values [16,17]. The samples were characterized by field-emission-gun scanning electron microscopy (FEG-SEM, Zeiss Supra 35 VP with an EDS analyzer) and transmission electron microscopy (TEM, Jeol JEM-2100 with $LaB_6$ cathode). The X-ray diffraction (XRD) spectra were analyzed on a X'Pert X-ray diffractometer. The IR spectra were obtained on a FTIR spectrometer (PerkinElmer 2000). The $N_2$ adsorption isotherms were measured using a Micromeritics ASAP 2020 Surface Area and Porosity Analyzer, and the BET surface area (SBET) was calculated from molecular cross-sectional area of analysis gas, the calculated slope and $y$-intercept of the least-squares fit performed on designated pairs of relative pressure and BET transformation. BET experiments were performed only for adsorption using nitrogen as adsorbate gas.

## 3. Results and discussion

### 3.1. Characterization

The samples prepared by the solvothermal process in a closed laboratory bottle and in an open reactor were characterized with FEG-SEM and TEM. Depending on the reaction parameters, i.e., synthesis technique, temperature, time, precursors and solutes, we obtained particles with very diverse morphologies, as presented in the FEG-SEM and TEM micrographs in Figs. 1 and 2, respectively. The micrographs illustrate the four different microstructures of the obtained particles. Sample A was prepared in a closed laboratory bottle in the precipitation of zinc nitrate with urea in water. The as-prepared particles have the typical micron-sized, flower-like morphology, as shown in the FEG-SEM and TEM micrographs in Figs. 1a and 2a, respectively. The smooth surface of the leaves, which make up the particles of sample A, is presented in the inset micrographs of Fig. 1a. The specific surface area of the sample A particles, measured with the BET method, was 13.5 $m^2\ g^{-1}$ (Table 1). The calculated average particle size from the XRD data (Fig. 3a), using the Sherrer equation, [19] was 20 nm. These small crystals

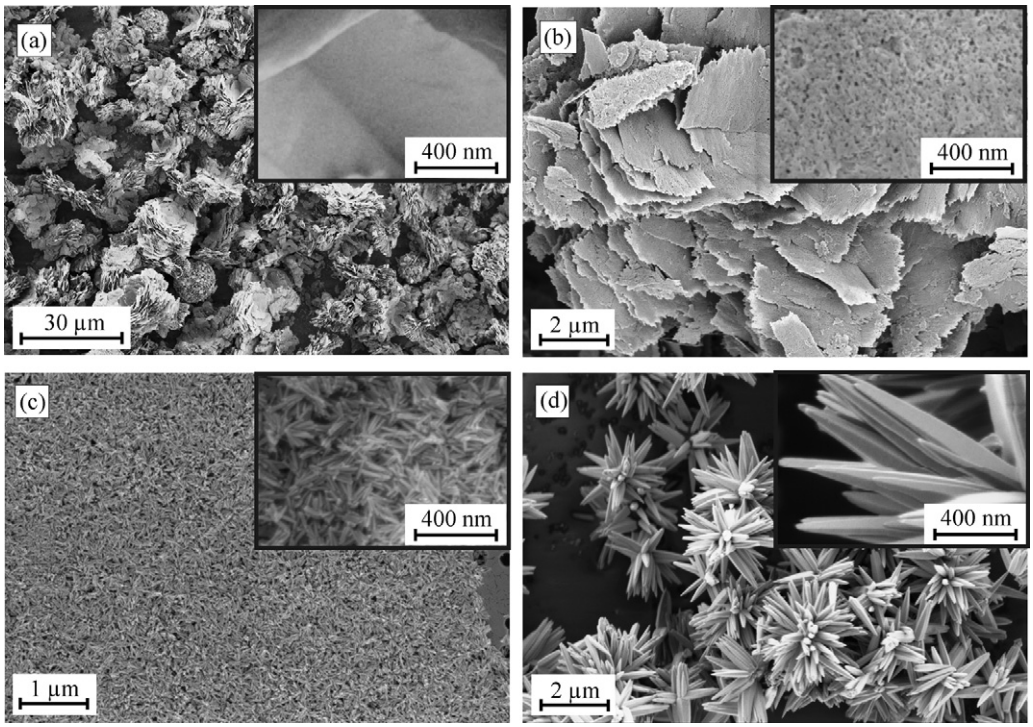


**Fig. 1.** FEG-SEM micrographs of (a) – Sample A, (b) – Sample TA, (c) – Sample B and (d) – Sample C.

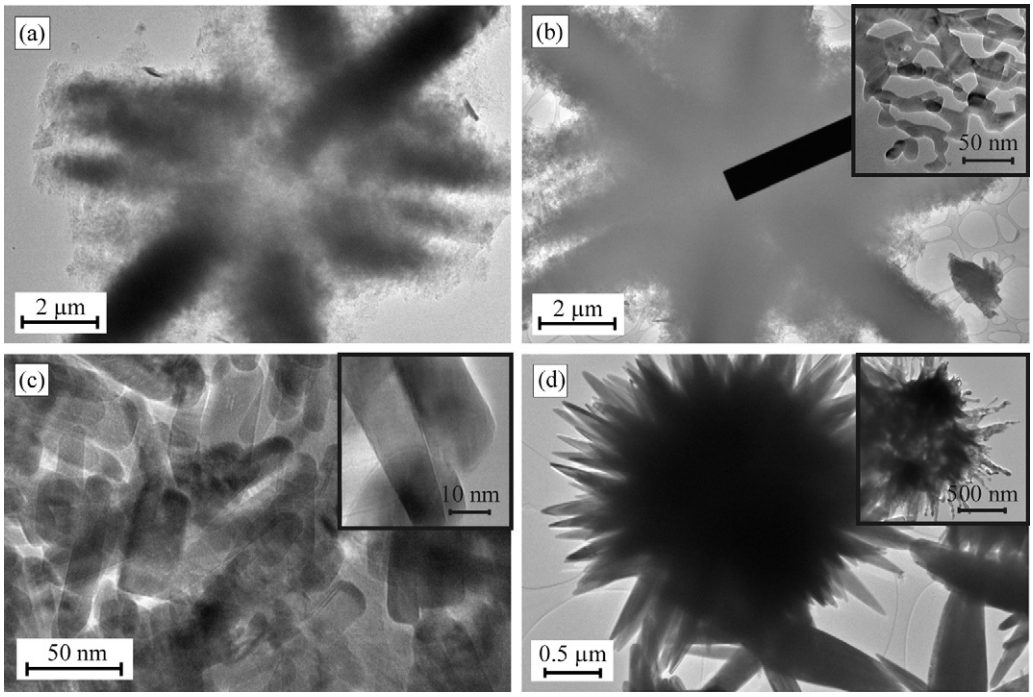


**Fig. 2.** TEM micrographs of (a) – Sample A, (b) – Sample TA, (c) – Sample B and (d) – Sample C.

**Table 1**
Specific surface area ($S$) for different catalysts used in this study.

| Catalyst | A | TA | B | C | P25 |
|---|---|---|---|---|---|
| $S_{BET}$ ($m^2\,g^{-1}$) | 13.5 | 61.3 | 55.4 | 4.0 | 53.0 |

formed aggregates with a diameter of 12.8 μm, estimated from the TEM micrographs. The determined energy gap was 4.1 eV.

Sample A was thermally treated at 300 °C for 1 h under a static atmosphere of air in order to prepare the ZnO particles (marked as sample TA). The particles kept their morphology on the microscale during the heat treatment, as presented in Figs. 1b and 2b. However, the annealing caused the formation of a nanoporous structure on

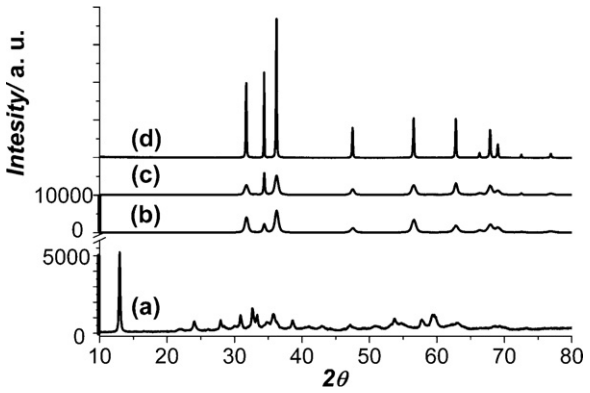


**Fig. 3.** XRD spectra of (a) – Sample A, (b) – Sample TA, (c) – Sample B and (d) – Sample C.

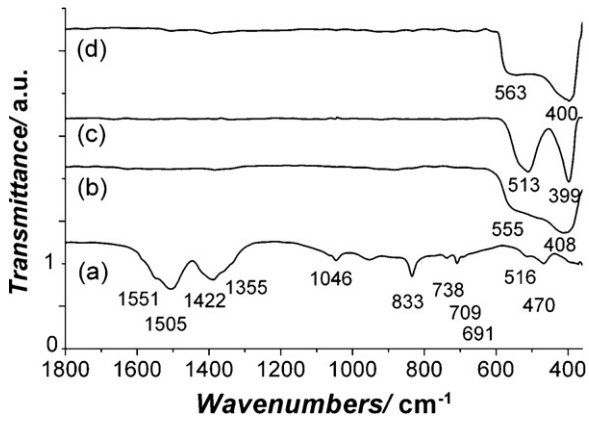


**Fig. 4.** FTIR spectra of (a) – Sample A, (b) – Sample TA, (c) – Sample B and (d) – Sample C.

the particles' surface (the inset in Figs. 1b and 2b), which resulted in an increase of the specific surface area to 61.3 $m^2\,g^{-1}$. The average particle size, calculated from the XRD data (Fig. 3b) using the Scherrer equation, was 40 nm, which is twice that of sample A, i.e., the crystals fused. However, the estimated average size of the aggregates was still 12.8 μm.

ZnO rod-like nanoparticles, marked as sample B, were prepared from zinc acetylacetonate and 1-butanole in a closed laboratory bottle. The as-prepared nanoparticles are presented in Fig. 1c. The length of the particles, estimated from the SEM and TEM micrographs, was about 70 nm and their width was about 15 nm. The nanoparticles' specific surface area was 55.4 $m^2\,g^{-1}$.

The particles of sample C have micron-sized, needle-like and, for ZnO, a typical, hexagonal morphology, as presented in Fig. 1d. The particles were prepared using a mixture of water and EG in an open reactor with constant stirring. The needle-like particles have grown together into up to 2.5-μm-large (estimated from the TEM and SEM micrographs), hedgehog-like particles, whose specific surface area was 4.0 $m^2\,g^{-1}$.

Samples TA and C exhibited a high sensitivity to the electron beam during the TEM examination. Even when using extremely mild conditions (the smallest condenser aperture and the smallest spot size possible), HRTEM imaging of sample TA was not possible (see inset in Fig. 2b), as the material deteriorated immediately. Sample C was stable under mild conditions, but could not withstand slightly harsher electron-beam conditions (see inset in Fig. 2d). On the other hand, the sample A, i.e., hydrozincite, and the sample B, i.e., rod-like ZnO, were relatively stable under the TEM electron beam (a spot size of 1 and the largest objective aperture).

All the prepared samples were characterized with XRD (Fig. 3) and FTIR (Fig. 4) spectroscopy. The XRD spectra of the samples A and TA are presented before and after the thermal decomposition in Fig. 3a and b respectively. The major peaks in the spectrum before the heat treatment (sample A, Fig. 3b) correspond to $Zn_5(OH)_6(CO_3)_2$ (JCPDS 19-1458). The low peak intensity and the slightly higher scattering background in the XRD pattern of the sample A confirmed that the product was not well crystallized. After the thermal decomposition (300 °C) in air, the sample A was transformed into the pure hexagonal ZnO phase (JCPDS 36-1451) of the sample TA (Fig. 3b). The XRD patterns of the samples B (Fig. 3c) and C (Fig. 3d) also correspond to the pure ZnO phase. The broader width of the peaks observed in the XRD spectra of the ZnO particles of samples TA and B indicated the presence of smaller particles, while the spectrum of the sample C corresponded to a well-crystallized ZnO structure.

The FTIR spectrum of sample A is presented in Fig. 4a. The presence of $CO_3^{2-}$ in the hydrozincite product was confirmed by the bands in the range from 1600 and 1200 $cm^{-1}$, and from 1000 to 680 $cm^{-1}$ [18]. After the thermal treatment of sample A at 300 °C, the band at 408 $cm^{-1}$ with a pronounced shoulder at 555 $cm^{-1}$ (Fig. 4b) confirmed the presence of the ZnO phase in sample TA. The ZnO phase was also detected in the FTIR spectra of the samples B and C, as presented in Fig. 4c and d, respectively.

### 3.2. Photocatalytic degradation of resazurin and caffeine

The photocatalytic activities of all the prepared samples were evaluated from the degradation of the resazurin and caffeine in an aqueous solution. The resazurin solution was violet-blue and was in contact with photocatalytic material which was exposed to UV radiation over a certain time. Resazurin's color changed upon photocatalysis, but not photolysis, to pink (resorufin). The process occurs quickly, making this test appropriate for "on the spot" investigations. On the other hand, the degradation of resazurin is complicated and limits the test to acidic pH, where the color change from violet to pink-orange happens in the range of pH between 3.8 and 6.4. To avoid the disadvantages of resazurin, the photocatalytic activities were also studied with caffeine Fig. 5.

The rate of conversion of resazurin and caffeine was monitored using UV–vis spectroscopy. Typical spectra of resazurin and caffeine are shown in Figs. 6 and 7, respectively. In addition to the experiments with the photocatalyst and irradiation, blank experiments in the presence of irradiation without the photocatalyst were also performed. The blank-experiment results showed that resazurin and caffeine could not be degraded without the photocatalyst. The relative concentration ($C/C_0$) of resazurin and caffeine

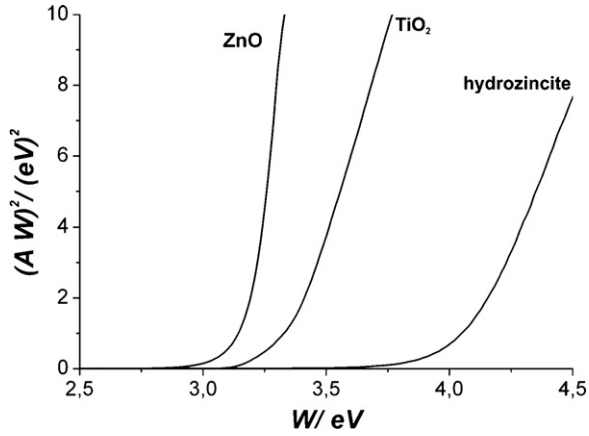


**Fig. 5.** Spectra for the band-gap determination of the ZnO materials, hydrozincite and $TiO_2$ (Degussa, P25).

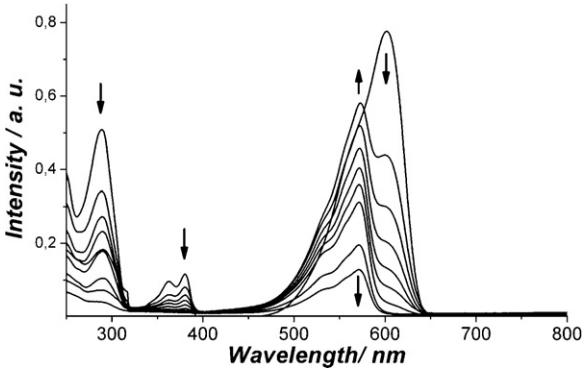


**Fig. 6.** A characteristic UV–vis spectra showing the photocatalytic degradation of resazurin. ZnO nanoparticles of sample C were used as a photocatalyst. The arrows indicate the direction of change.

were determined from the corresponding peaks in the UV/vis spectra at approximately 600 nm and 270 nm, respectively. First, the baseline was created and subtracted; second, the deconvolution of the peaks was performed because of the partial overlapping with the resorufin peak (in the case of resazurin) or baseline drift (in the case of caffeine) (Gaussian peak function was fitted onto measured spectra fixing the offset at 0, the center at peak maximum, the amplitude at maximal absorbance, and regressing the width); and third, the obtained peaks were integrated and normalized to the initial peak area (concentration).

Since the concentration of caffeine was measured by UV–vis spectroscopy at 270 nm, possible reaction intermediates exhibiting absorbance in the same wavelength range and affecting the determined concentrations of caffeine have to be considered. These intermediates are adsorbed onto the catalyst surface until simple molecules, such as $H_2O$ and $CO_2$, are formed. Thus one only has to take into account that the determined reaction rate constant of photocatalysis is the one pertinent to the rate-determining step of the process and not necessarily the one related to the decomposition of caffeine to the first reaction intermediate in a series of subsequent reactions of its decomposition. One has to be aware that that intermediates could be desorbed and also that the reaction with hydroxyl (or other) radicals could occur in liquid phase. Nonetheless, no intermediates could be detected within the examined range of UV–vis spectra; consequently, they presumably remain adsorbed, while the reaction with hydroxyl (or other) radicals in the liquid phase may be considered negligible in extent

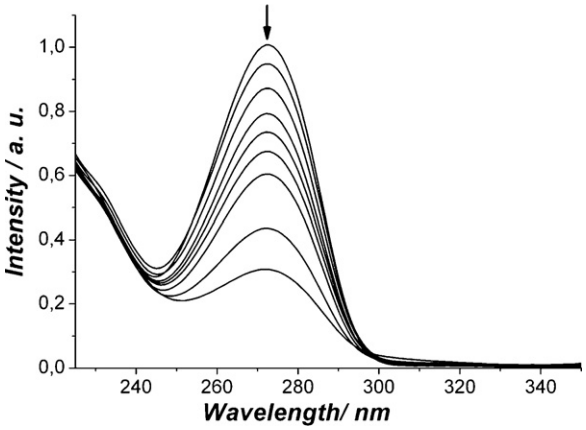


**Fig. 7.** Characteristic UV–vis spectra showing the photocatalytic degradation of caffeine. ZnO nanoparticles of sample C were used as a photocatalyst. The arrows indicate the direction of change.

**Table 2**
Observed first-order, second-order and Langmuir–Hinshelwood rate constants for the degradation of aqueous caffeine upon UV–vis irradiation; $C_0 = 4.89 \times 10^{-3}$ wt.% (caffeine); $C_S = 0.2 - 1.2\ g\,L^{-1}$ (ZnO); air atmosphere.

| TA Primary use | $C_S = 0.2\ g\,L^{-1}$ | $C_S = 0.4\ g\,L^{-1}$ | $C_S = 0.8\ g\,L^{-1}$ | $C_S = 1.2\ g\,L^{-1}$ |
|---|---|---|---|---|
| $k_1$ ($10^{-3}$ min$^{-1}$) | 1.15 ± 0.10 | 1.85 ± 0.08 | 2.14 ± 0.04 | 2.29 ± 0.06 |
| $R^2$ | 0.898 | 0.982 | 0.994 | 0.991 |
| $k_2C_0$ ($10^{-3}$ min$^{-1}$) | 1.22 ± 0.10 | 2.02 ± 0.07 | 2.36 ± 0.03 | 2.54 ± 0.05 |
| $R^2$ | 0.908 | 0.987 | 0.997 | 0.992 |
| $k_3K$ ($10^{-2}$ min$^{-1}$) | 0.73 ± 0.06 | 1.15 ± 0.05 | 1.31 ± 0.02 | 1.39 ± 0.04 |
| $K$ ($10^3$ wt.%$^{-1}$) | 1.16 ± 0.05 | | | |
| $R^2$ | 0.889 | 0.977 | 0.989 | 0.983 |

| TA $C_S = 0.4\ g\,L^{-1}$ | Primary use | Secondary use | Tertiary use |
|---|---|---|---|
| $k_1$ ($10^{-3}$ min$^{-1}$) | 1.85 ± 0.08 | 1.72 ± 0.03 | 1.64 ± 0.06 |
| $R^2$ | 0.982 | 0.995 | 0.983 |
| $k_2C_0$ ($10^{-3}$ min$^{-1}$) | 2.02 ± 0.07 | 1.86 ± 0.02 | 1.77 ± 0.05 |
| $R^2$ | 0.987 | 0.998 | 0.989 |
| $k_3K$ ($10^{-2}$ min$^{-1}$) | 1.15 ± 0.05 | 1.07 ± 0.02 | 1.02 ± 0.04 |
| $K$ ($10^3$ wt.%$^{-1}$) | 1.16 ± 0.05 | | |
| $R^2$ | 0.977 | 0.991 | 0.977 |

| $C_S = 0.4\ g\,L^{-1}$ Primary use | A | TA | B | C | P25 |
|---|---|---|---|---|---|
| $k_1$ ($10^{-3}$ min$^{-1}$) | / | 1.85 ± 0.08 | 8.3 ± 0.2 | 1.37 ± 0.07 | 37 ± 3 |
| $R^2$ | | 0.982 | 0.995 | 0.961 | 0.976 |
| $k_2C_0$ ($10^{-3}$ min$^{-1}$) | / | 2.02 ± 0.07 | 11 ± 1 | 1.44 ± 0.07 | 70 ± 10 |
| $R^2$ | | 0.987 | 0.971 | 0.969 | 0.913 |
| $k_3K$ ($10^{-2}$ min$^{-1}$) | / | 1.15 ± 0.05 | 1.82 ± 0.04 | 0.91 ± 0.05 | 21 ± 2 |
| $K$ ($10^3$ wt.%$^{-1}$) | | 1.16 ± 0.05 | 0.329 ± 0.008 | 1.22 ± 0.06 | 1.70 ± 0.10 |
| $R^2$ | | 0.977 | 0.997 | 0.953 | 0.999 |

due to extremely low degradation rate in the absence of catalyst, as described above.

The overall decomposition rate of the resazurin or caffeine is determined by the diffusional resistance around the photocatalyst particles (external mass transfer) and the surface reaction kinetics.

In order to confirm the absence of the external mass-transfer resistance, the rotational speed was varied for sample TA at 0.4 g L$^{-1}$ of ZnO that is the rotational speeds of 600, 650, 700, 750, and 800 rpm were tested and no differences were observed. Fig. 8a shows that there is no difference in the decomposition rate upon the utilization of the rotational speeds of 750 and 800 rpm. Neglecting the hydrodynamic effects [7,8,11–13] or the relatively low rotational speed (70 rpm) [9,10] may in turn result in apparent reaction-rate constants, influenced by the external mass transfer. In contrast, intensive mixing (600 rpm [14] or 1200 rpm [15]) decreases the external mass-transfer resistance. Nevertheless, its absence has to be confirmed by the rotational speed variation for different impellers and reactor geometries.

The first-order ($k_1$ in Eq. (1)), second-order ($k_2$ in Eq. (2)) and Langmuir-Hinshelwood ($k_3$ in Eq. (3), $K$ is the equilibrium constant) reaction-rate constants were determined from the following expressions using nonlinear regression (Levenberg–Marquardt algorithm, $10^{-5}$ tolerance) and are reported in Tables 2 and 3 for caffeine and resazurin, respectively. These different models were used, as they are all mentioned in the literature to represent the obtained experimental results of photocatalysis process [8–15].

$$\frac{dC}{dt} = -r = -k_1 C \quad (1)$$

$$\frac{dC}{dt} = -r = -k_2 C^2 \quad (2)$$

$$\frac{dC}{dt} = -r = -\frac{k_3 K C}{1 + KC} \quad (3)$$

Fig. 8b shows that the caffeine concentration decreases at a faster rate with an increase of the ZnO load, which is clear from

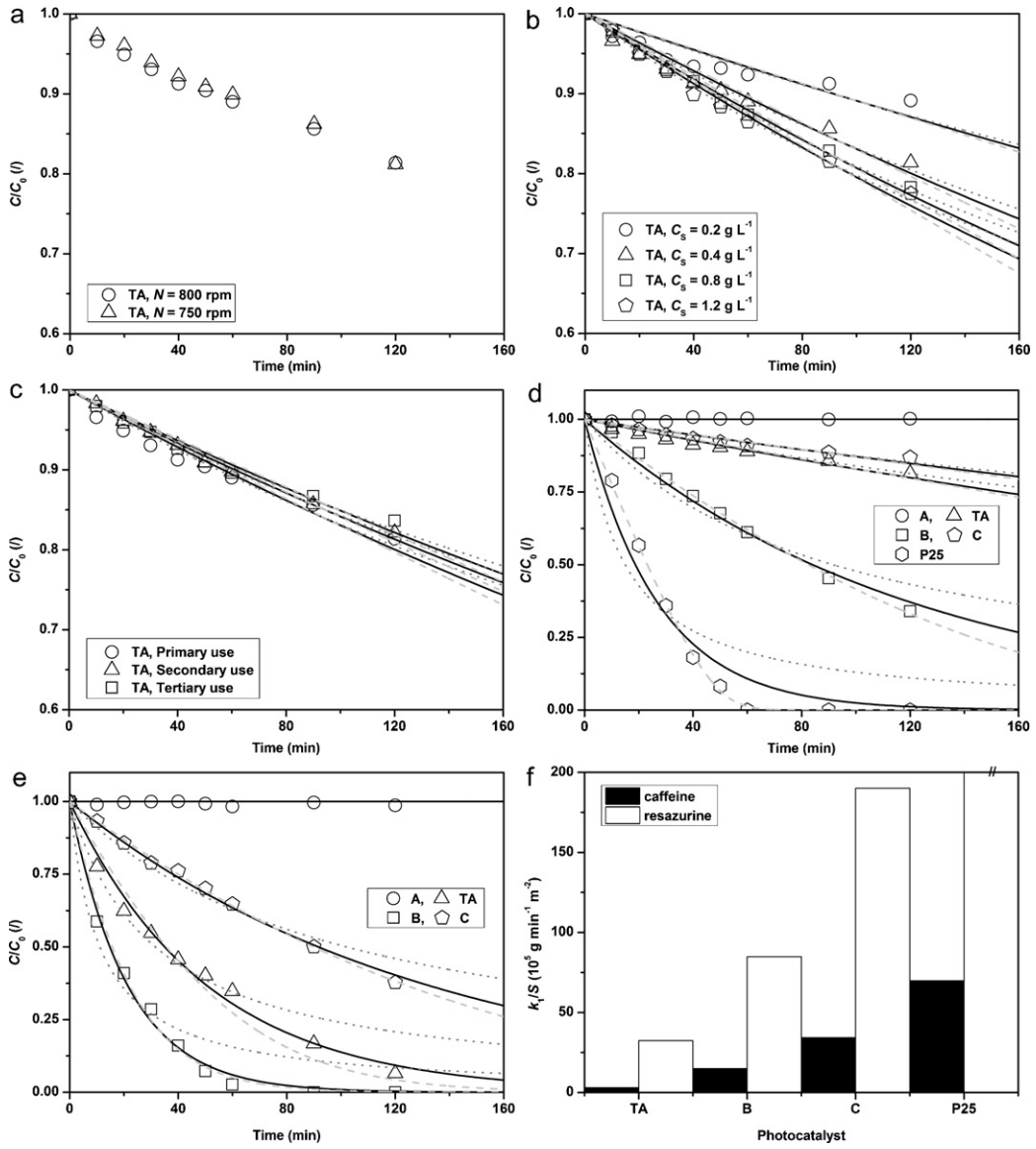


**Fig. 8.** Comparison of the degradation of aqueous caffeine upon irradiation at different rotational speeds (a), first-order (------), second-order (.....) and Langmuir–Hinshelwood (-- -- --) kinetics for different photocatalyst loads (caffeine degradation) (b), multiple photocatalyst use (caffeine degradation) (c), material and photocatalyst morphology (caffeine degradation) (d), material and photocatalyst morphology (resazurin degradation) (e), and comparison of reaction-rate constants per specific surface area for different photocatalyst morphologies (f).

the increasing reaction-rate constants of all the kinetic models in Table 2. There are no major differences between the three utilized models as the decrease is basically linear. The Langmuir–Hinshelwood model reflects the real mathematical relationship of the kinetics of the photocatalytic reaction, since the reactant (resazurin or caffeine) bonds to an adsorption site on the surface (ZnO or $TiO_2$) (first step), where it reacts with the reaction rate constant $k_1$ (second step). Small differences between models (Fig. 8b and c) at small extents of degradation may be mathematically explained with $-r \approx -r_0$ when $C \approx C_0$ that is at small extents of degradation, the degradation rate is approximately constant, regardless of the utilized model. At large extents of degradation, small differences between models (Fig. 8d, samples B and P25, and Fig. 8e, samples TA, B and C) pertain only to the Langmuir–Hinshelwood and first-order models and may be mathematically explained with $k_1 \approx k_3 K$ when $KC \ll 1$ that is at large extents of degradation the degradation rate is approximately first-order. Low $R^2$ values for the second-order model at large extents of degradation in turn confirm the adequacy of the Langmuir–Hinshelwood model or its approximation, the first-order model, which may be checked by comparing Fig. 8d and e with Tables 2 and 3 for samples B ($R^2 = 0.971$) and P25 ($R^2 = 0.913$) (caffeine), and TA ($R^2 = 0.970$) and B ($R^2 = 0.968$) (resazurin), respectively.

**Table 3**
Observed first-order, second-order and Langmuir–Hinshelwood rate constants for the degradation of aqueous resazurin upon UV–vis irradiation; $C_0 = 1.06 \times 10^{-3}$ wt.% (resazurin); $C_S = 0.4\,g\,L^{-1}$ (ZnO); air atmosphere.

| $C_S = 0.4\,g\,L^{-1}$ Primary use | A | TA | B | C | P25 |
|---|---|---|---|---|---|
| $k_1$ ($10^{-2}$ min$^{-1}$) | / | $1.98 \pm 0.07$ | $4.7 \pm 0.3$ | $0.76 \pm 0.01$ | Inst.[a] |
| $R^2$ | | 0.990 | 0.994 | 0.995 | |
| $k_2 C_0$ ($10^{-2}$ min$^{-1}$) | / | $3.2 \pm 0.6$ | $9 \pm 2$ | $0.98 \pm 0.08$ | Inst.[a] |
| $R^2$ | | 0.970 | 0.968 | 0.976 | |
| $k_3 K$ ($10^{-2}$ min$^{-1}$) | / | $3.5 \pm 0.1$ | $5.5 \pm 0.4$ | $1.18 \pm 0.02$ | Inst.[a] |
| $K$ ($10^3$ wt.%$^{-1}$) | | $1.07 \pm 0.04$ | $0.32 \pm 0.02$ | $0.692 \pm 0.009$ | |
| $R^2$ | | 0.984 | 0.994 | 0.998 | |

[a] Instantaneous reaction.

The deviation from the ideal agreement may be due to the aggregation of free catalyst particles and the "screening" effect [14]. Vora et al. [7] and Yatmaz et al. [14] also noted an increase of the reaction-rate constant with ZnO load, and the second group established the proportionality of the constant and $C_S^{0.6}$. The exponent in this study was determined as 0.37, 0.40, and 0.35 for the first-order, second-order, and Langmuir-Hinshelwood reaction-rate constants, respectively. The exponents were determined as the slope in the log-log plots of $k_1$, $k_2C_0$, and $k_3K$ versus $C_S$ for the three mentioned kinetic models (*e.g.* the formula between $k_1$ and $C_S$ as its main influencing factor being $k_1 = k_{10}C_S^n$). This was done in order to determine the dependency of the degradation rate on catalyst load for the prediction and optimization of the necessary ZnO catalyst load for a demanded degradation rate in an application. The observed increase would normally reverse after the optimal photocatalyst load as the increase in the load of the catalyst has two opposite contributions to the degradation process [8–13]. A larger number of active sites are available for the adsorption on the surface of particles. The amount of light that is dispersed by the catalyst particles is higher [8]. From the asymptotic dependency of the reaction rate constants on the ZnO load, 1.2 g $L^{-1}$ may be considered as the optimum load, as the constants to a large extent ceased to vary with the ZnO concentration increase.

Another important feature of a photocatalyst is an ability to withstand deactivation. This can be investigated by multiple catalyst use; however, this is seldom looked at despite the importance of photocatalyst recycling [7,8,11,12,14,15]. Deactivation most often occurs because of reaction intermediates and products that are irreversibly adsorbed onto the photocatalyst surface and thus decrease the number of active reaction sites [11]. Fig. 8c reveals that there is a certain extent of catalyst deactivation, although it is rather small. Moreover, the reaction-rate constants imply that the deactivation should not be complete even after several cycles of use. By applying a power-law relationship, the reaction-rate constants after 100 cycles of use would retain 60.5%, 57.5%, and 60.6% of their initial values for the first-order, second-order, and Langmuir–Hinshelwood reaction-rate constants, respectively.

The apparent linear decrease of $C/C_0$ versus time in Fig. 8a–c suggests a zero-order kinetics model (instead of other models), which is normally found in advanced oxidation processes when the organic charge in the system is high (the concentration of caffeine is quite high, namely $4.89 \times 10^{-3}$ wt.%). Nonetheless, the utilization of the zero-order reaction rate equation model did not improve the agreement between measured and predicted data. What is more, other ZnO morphologies (Fig. 8d and e) visibly deviated from zero-order kinetics model. The latter may only be concluded based on the assumption that the basic mechanism of the photocatalytic decomposition of caffeine (Fig. 8d) and resazurin (Fig. 8e) on either ZnO or $TiO_2$ is analogous, which was indeed shown for different components [7–15]. What is more, one has to assume that different ZnO morphologies (Fig. 8d) do not lead to different intrinsic reaction kinetics (different catalytic material), but merely to different global kinetics of reactions due to varying internal mass transfer resistance (different effective diffusion within catalyst particles); nonetheless, this is not necessarily the case.

The influence of the ZnO morphology on the photocatalytic decomposition of caffeine and resazurin is presented in Fig. 8d and e, with the corresponding reaction-rate constants in Tables 2 and 3, respectively. A general observation is that resazurin reacts much faster than caffeine with all the catalysts, especially with the reference $TiO_2$ (Degussa P25), which almost instantly decolorizes the aqueous resazurin. Hydrozincite (sample A) does not exhibit any photocatalytic activity, either for caffeine or resazurin, due to the much larger band gap compared to ZnO, i.e., 4.1 eV for hydrozincite and 3.2 eV for all the prepared ZnO samples. The thermally treated sample A, i.e., TA, exhibits some photocatalytic activity, while sample A does not show any photocatalytic effect.

Fig. 8f provides an intriguing comparison of the first-order reaction-rate constant per specific surface area for all the employed photocatalysts. The activity of $TiO_2$ is superior by far, but ZnO represents a fairly good alternative due to the cost efficiency of its production, thus the cost argument is much better. This affirmation may be reinforced by a simple cost analysis, that is the market price of nano-$TiO_2$ (176–198 $/kg) is much higher than that of nano-ZnO (1.5 $/kg) [20,21]. The most interesting observations may be drawn from a comparison of samples A, B, and C. Samples B and C have a similar needle-like morphology (Fig. 1c and d), though the crystal size is much smaller and hence the specific surface area is much larger for sample B. Thus the reaction-rate constants and the extent of the decomposition are greater overall, although the specific activity (Fig. 8f) may be lower because of the greater internal mass-transfer resistance, as the surfaces of the larger ZnO crystals (C) are more exposed to the caffeine or resazurin diffusional flux (Fig. 1c and d). In addition, there is bound to be a larger degree of agglomeration in sample B, which renders some of the catalytic surface less accessible to the component being decomposed. This phenomenon is even more pronounced for samples A, where the diffusional resistance in nanosized pores (Fig. 1b) is even larger. All the reaction-rate constants in Tables 2 and 3 thus encompass the intrinsic kinetics and the internal mass transfer, and should be considered as apparent. Nevertheless, they represent a relatively good criterion for photocatalytic activity.

The morphology of ZnO photocatalyst affects its activity (Fig. 8f) and the reasons why the morphology has such influence may be sought in physical and chemical processes underlying the overall degradation process. Beside the mentioned explanation concerning a greater internal mass-transfer resistance (diffusion as a physical process), the catalyst surface may also be inactive due to an inadequate thermal treatment or contamination by (Section 2.1 *ZnO preparation*) (photocatalytic reaction as a chemical process), *e.g.* a portion of the catalyst in the sample TA may be present in the form of inactive hydrozincite thus lowering the catalytic activity of the sample TA, even though hydrozincite is not detected by XRD in Fig. 3. There may also be acetylacetonate contamination in the less accessible parts among the rods of sample B, which can account for lower specific activity of the sample B in comparison to C.

The reaction mechanism for the conversion of caffeine to dimethylparabanic acid involves initially the (fast) attack of hydroxyl radicals to the C4=C8 double bond of caffeine, and after successive hydroxylations and oxidations, 1,3-dimethyl-2,4,5-tricarboxyimidazolidine (dimethylparabanic acid) and 1,3-dihydroxymethyl-2,4,5-tricarboxyimidazolidine are formed, whereas 1,3-dihydroxymethyl-2,4,5-tricarboxyimidazolidine is slowly mineralized to $CO_2$, $NH_3$, and $NH_2Me$ [22]. The main intermediates formed are thus 4,8-dihydroxyl-added caffeine, dimethylparabanic acid and 1,3-dihydroxymethyl-2,4,5-tricarboxy imidazolidine, and the obtained photoproducts carbon dioxide, ammonia, and methylamine [22]. The rate of evolution (generation/disappearance) of the main intermediates formed is fast; [22] consequently, the rate of desorption is much slower than the reaction rate of the conversion of these intermediates, which predominantly remain adsorbed to photocatalyst surface and were not detected in the liquid phase. $K$ and $k_3$ of Langmuir-Hinshelwood model therefore correspond to the caffeine adsorption equilibrium constant and the reaction rate constant of the rate-determining step of mineralization. The reaction mechanism for the conversion of resazurin is its initial photoreduction to resorufin, which bleaches upon further irradiation with UV light [23]. The

photobleaching process is associated with the further reduction of the dye, the most obvious product is dihydroresorufin, but the latter is oxygen-sensitive, and so the initial pink coloration due to resorufin should recover if the photobleached film is left in the dark [23]. The main intermediates formed are thus resorufin and dihydroresorufin, and the obtained photoproducts carbon dioxide, ammonia, and volatiles [23]. The reasoning, analogous to photocatalytic decomposition of caffeine, may be applied for resazurin.

## 4. Conclusion

The impact of the surface morphology of particles on the photocatalytic properties was investigated for various materials with their corresponding morphologies, such as micron-sized and flower-like particles of hydrozincite ($13.5\,m^2\,g^{-1}$), micron-sized aggregates of 20-nm-large ZnO nanoparticles ($61.3\,m^2\,g^{-1}$), approximately $70 \times 15$ nm ZnO nanorods ($55.4\,m^2\,g^{-1}$), up to 2.5-μm-sized hedgehog-like ZnO particles ($4.0\,m^2\,g^{-1}$) and $TiO_2$ (P25) ($53.0\,m^2\,g^{-1}$), which served as a reference. The estimated direct bad gap for the ZnO particles was 3.2 eV, 3.3 eV for the $TiO_2$ (P25), and 4.1 eV for the hydrozincite. The last of these was not determined before, to the best of our knowledge.

The degradation of the resazurin and caffeine was monitored by UV–vis spectroscopy for the evaluation of the photocatalysis kinetics. The absence of an external mass-transfer resistance was first confirmed by the differing rotational speed, which did not affect the apparent resazurin and caffeine degradation rate. Consequently, first-order, second-order and Langmuir–Hinshelwood kinetics were applied to the experimental data. Moreover, the synthesized ZnO proved to be a fairly stable catalyst as its repeated use only resulted in a limited decrease of catalyst activity. Furthermore, the material can presumably be reactivated with a thermal treatment following extensive deactivation. We found that the activity of $TiO_2$ is superior, but ZnO represents a good alternative, due to the cost efficiency of its production, especially material prepared by a solvothermal procedure in water and ethylene glycol (sample C), which had the highest degradation rate per specific surface of material, i.e., the degradation-rate constants per specific surface area were 34 and $190 \times 10^5\,g\,min^{-1}\,m^{-2}$ for the caffeine and resazurin, respectively.

## Acknowledgment

The authors gratefully acknowledge the financial support of the Ministry of Higher Education, Science and Technology of the Republic of Slovenia through the contract No. 3211-10-000057 (Center of Excellence for Polymer Materials and Technologies), and the Slovenian Research Agency (programme P1-0030, P2-0152 and Grant No. 1000-08-310086).

## References

[1] J.A.R. Marquez, C.M.B. Rodriguez, C.M. Herrera, E.R. Rosas, O.Z. Angel, O.T. Pozos, International Journal of Electrochemical Science 6 (2011) 4059–4069.
[2] Y.L. Lai, M. Meng, Y.F. Yu, X.T. Wang, T. Ding, Applied Catalysis B Environmental 105 (2011) 335–345.
[3] D. Reyes-Coronado, G. Rodriguez-Gattorno, M.E. Espinosa-Pesqueira, C. Cab, R. de Coss, G. Oskam, Nanotechnology 19 (2008) 1–10.
[4] D. Li, H. Haneda, Chemosphere 51 (2003) 129–137.
[5] K. Byrappa, A.K. Subramani, S. Ananda, K.M.L. Rai, R. Dinesh, M. Yoshimura, Bulletin of Materials Science 29 (2006) 433–438.
[6] J.L. Yang, S.J. An, W.I. Park, G.C. Yi, W. Choi, Advanced Materials 16 (2004) 1661–1664.
[7] J.J. Vora, S.K. Chauhan, K.C. Parmar, S.B. Vasava, S. Sharma, L.S. Bhutadiya, European-Journal of Chemistry 6 (2009) 531–536.
[8] C. Martinez, M. Canle, M.I. Fernandez, J.A. Santaballa, J. Faria, Applied Catalysis B Environmental 102 (2011) 563–571.
[9] A.N. Rao, B. Sivasankar, V. Sadasivam, Journal of Molecular Catalysis A – Chemical 306 (2009) 77–81.
[10] A.N. Rao, B. Sivasankar, V. Sadasivam, Journal of Hazardous Materials 166 (2009) 1357–1361.
[11] M.A. Behnajady, N. Modirshahla, R. Hamzavi, Journal of Hazardous Materials 133 (2006) 226–232.
[12] K. Djebbar, T. Sehili, Pesticide Science 54 (1998) 269–276.
[13] S. Chakrabarti, B.K. Dutta, Journal of Hazardous Materials 112 (2004) 269–278.
[14] H.C. Yatmaz, A. Akyol, M. Bayramoglu, Industrial and Engineering Chemistry Research 43 (2004) 6035–6039.
[15] K.V. Kumar, K. Porkodi, A. Selvaganapathi, Dyes and Pigments 75 (2007) 246–249.
[16] A.E. Jimenez, S.G. Santiago, Semiconductors Science and Technology 22 (2007) 709–719.
[17] Z. Crnjak Orel, B. Orel, Physical Status Solidi B 186 (1994) K33–K36.
[18] M. Bitenc, M. Marinšek, Z.C. Orel, Journal of the European Ceramic Society 28 (2008) 2915–2921.
[19] P. Scherrer, Göttinger Nachrichten. Mathematical Physics 2 (1918) 98–100.
[20] C.O. Robichaud, A.E. Uyar, M.R. Darby, L.G. Zucker, M.R. Wiesner, Environmental Science and Technology 43 (2009) 4227–4233.
[21] http://www.researchandmarkets.com, accessed October 2012
[22] I. Dalmazio, L.S. Santos, R.P. Lopes, M.N. Eberlin, R. Augusti, Environmental Science and Technology 39 (2005) 5982–5988.
[23] A. Mills, J.S. Wang, M. McGrady, Journal of Physical Chemistry B 110 (2006) 18324–18331.